Voltage and Frequency control of standalone 1-ϕ Microgrid Using Adaptive Sliding Mode Control Algorithm (ASMCA)

P. Harish, I. Kumara swamy, N.Gireesh

Abstract— In this contribution, 1-ϕ standalone microgrid configuaration using hydro, wind, solar and Battery Energy Storage System (BESS), all those generating sources interconnecting one 1-ϕ Voltage Source Converter (VSC). The VSC controls with the assistance of Adaptive Sliding Mode Control Algorithm (ASMCA). The ASMCA is utilized to assess the reference source current which controls the VSC and regulates the voltage and frequency of the microgrid in addition to harmonics current extenuation and power balance is found highly suitable, stable and robust for such highly nonlinear micro-grid system, and also It is well known that the dynamic variation of solar insolation levels and sudden variation of wind speeds to maintain the PCC voltage at reference value. Proposed microgrid results are analyse in MATLAB/SIMULINK.

Index Terms—Hybrid microgrid systems, ASMCA, BESS.

1 Introduction

THE amalgamation of non-conventional energy sources like wind, PV and conventional energy source such as hydro with Battery Energy Storage System are presently well predictable. The utility of microgrid as controlled entities reconnoiters the possibility of organizing standalone non-conventional energy sources so that they behave as a single manufacturer of electrical energy to reward the full benefits of non-conventional energy sources in a reliable and adaptable way. The balance of electrical energy and system parameter control are the important features of the microgrid.

The growth of operative frequency and control of voltage scheme is essentially desired in order to achieve proper integration of non-conventional energy sources (NCES) [1] - [2]. Depending upon the development of appropriate control arrangement, a microgrid is having competence to activate in both standalone as well as grid tied modes of operation [3] - [4]. In grid tied microgrid, the central grid supplies the discrepancy power and absorbs the excess power in a grid tied microgrid system in order to sustain power balance which in turn controls the system frequency. Whereas, in a standalone microgrid, the balance of active and reactive powers, is attained using controlling the power flow among the various components of the microgrid [5] - [6]. The voltage, frequency, true and reactive powers are the main system parameters required to control the operation of the microgrid [6]. Battery Energy Storage System allows the large scale amalgamation of erratic energy sources [6]. In spite of its assistances, the capacity of Battery Energy Storage System is not abundantly consumed in the microgrid system so far [8]. Power electronic control of cohesive non-conventional systems has been deliberated broadly in [9] - [10]. The main task in control of standalone microgrid comprises the power balance and system voltage control [11]. Normalized adaline based control algorithm and other control schemes of 1-ϕ self-excited induction generator serving fluctuating loads is stated in [12]-[17]. The contrast among PV array MPPT methods are deliberated in [18]. In this work, the design and implementation of ASMCA [19] of 1-ϕ microgrid system is projected. It consists of three main non-conventional energy sources such as micro-hydro, wind and solar PV based generation.

2 Hybrid Microgrid Generation

2.1 Micro Hydro Power Generation (MHPG)

In MHPG the kinetic energy developed due to gravity in a falling water from upper to lower head is utilized to rotate a turbine to generate electrical power.

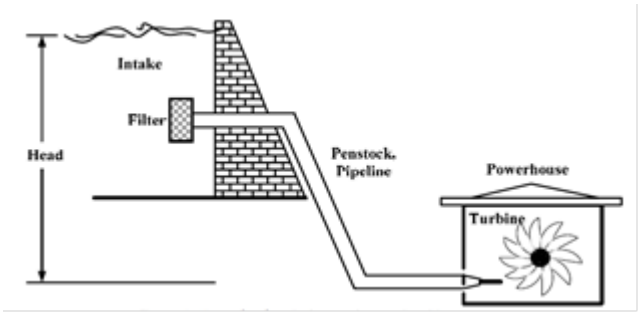

Fig. 1. Micro hydro generation configuration

The energy is extracted from the water depends on the volume and on the difference in height between the source and the water outflow, which is called the head. In order to get very large head, water for a hydraulic turbine may be run through a large pipe called a penstock, shown in Fig. 1.

Per unit turbine flow in terms of water time constant and head.

$$\frac{dq}{dt} = \left((h_s - h - h_l) \frac{gA}{L} \right) \quad (1)$$

Where,

- *P. Harish currently pursuing M-TECH in electric power systems in SVEC, Tirupati, and Andhra Pradesh PH-9052684346. E-mail: pasupuletiharish222@gmail.com*
- *I. Kumaraswamy, Assistant Profeser of EEE, SVEC, Tirupati, and Andhra Pradesh, PH-9985015365. E-mail: kumarswamy04@gmail.com*
- *N. Gireesh, Professor of ECE, SVEC, Tirupati, and Andhra Pradesh*

Applied Renewable energy Research Lab

q = per-unit water discharge

h_s = static head of the water column

h = head at the turbine admission

h_l = per-unit conduit head losses

L = length of the conduit section

A = cross section area of the penstock

g = gravitational force

The function of flow and toque of Francis turbine are given by Equation 2 and 3

$$Q = Q(H, x, y) \quad (2)$$

$$M_t = M_t(H, x, y) \quad (3)$$

Where
Q = flow rate
Mt = turbine torque
H = hydro-turbine water head
Y= gate opening
x = hydro turbine speed.

When the parameters of turbine vary in the small range at a stable operating point, the above two functions for water flow and toque can be linearized (Equation 4 and 5) as:

$$q = e_{qy} y + e_{qx} x + e_{qh} h \quad (4)$$

$$M_t = e_y y + e_x x + e_h h \quad (5)$$

$e_y = \frac{\partial m_t}{\partial y}$, Partial derivative of the torque to gate opening

$e_x = \frac{\partial m_t}{\partial x}$, Partial derivative of the torque to speed of turbine

$e_h = \frac{\partial m_t}{\partial h}$, Partial derivative of the torque to water head of turbine

$e_{qy} = \frac{\partial q}{\partial y}$, Partial derivative of flow to gate opening

$e_{qx} = \frac{\partial q}{\partial x}$, Partial derivative of flow to speed of the turbine

$e_{qh} = \frac{\partial q}{\partial h}$, Partial derivative of flow to the head of turbine

The developed power, Pm in turbine can be written as

$$P_m = A_t H(Q - Q_{nl}) \quad (6)$$

Where, A_t is the turbine gain, Q_{nl} is the no load flow rate.

The load impedance model of SEIG can be expressed as follow,

$$\frac{di_{Ld}}{dt} = \frac{1}{L_l}\left(V_{ds} - R_l i_{Ld}\right) + \omega_S i_{Ld} \quad (7)$$

$$\frac{di_{Lq}}{dt} = \frac{1}{L_l}\left(V_{qs} - R_l i_{Lq}\right) + \omega_S i_{Lq} \quad (8)$$

The excitation capacitor model can be expressed as,

$$\frac{dV_{ds}}{dt} = \frac{-1}{C} i_{ds} + \frac{1}{C} i_{Ld} \quad (9)$$

$$\frac{dV_{qs}}{dt} = \frac{-1}{C} i_{qs} + \frac{1}{C} i_{Lq} \quad (10)$$

2.2 Wind Power Generation

The wind energy conversion systems are acclimated to convert wind energy into different forms of electrical energy utilizing a wind turbine and a potency conversion.

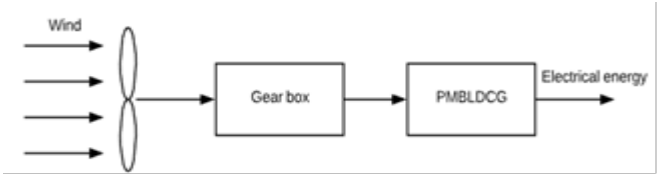

Fig. 2. System configuration for micro wind generating system

As shown above Fig.2 the basic parts of micro wind systems are,
Gearbox – to regulate the speed to required manner.
Boost converter – to stepping up voltage.
Alternator or generator - to transform the rotational energy into electricity.

Wind turbine mechanical power

$$P_t = 0.5 C_p(\lambda, \beta) \rho A V_w^3 \quad (11)$$

$$C_p(\lambda, \beta) = C1.\left[\frac{C2}{\lambda i} - C3.\beta - C4\right].e^{\frac{-C5}{\lambda_i}} + C6 \quad (12)$$

Where
P = the air density (kg/m3)
A = the area swept by turbine-rotor blades
V_w = the wind speed
C_p = the power coefficient of the turbine
C1=0.5176,
C2=116,
C3=0.4,
C4=5,
C5=-21,
C6=0.0068.

$$\omega_r = \frac{\lambda_{opt}}{R_t} V_w \quad (13)$$

$$P_{\max} = \frac{1}{2}.\pi.R_t.\rho_{air}.\frac{C_{p\max}.\lambda_{opt}^3.V_w^3}{\lambda_{opt}^3.R_t} \quad (14)$$

$$P_{\max} = K_{optim}\omega_r^3 \quad (15)$$

2.3 PV Generation

Converting solar energy to electricity energy by use of photo-voltaic cell is key element to get energy supply for our society profitable in the future. This energy can be network associated or it can be disengaged or independent power creating framework that relies upon the utility, area of load region, availability of power grid nearby it.

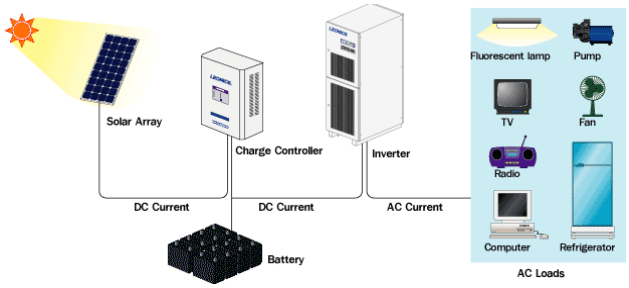

Fig. 3. Standalone-PV generator system

In standalone PV generator system the charge controller helps to predict overcharging of a battery as shown in Fig.3.

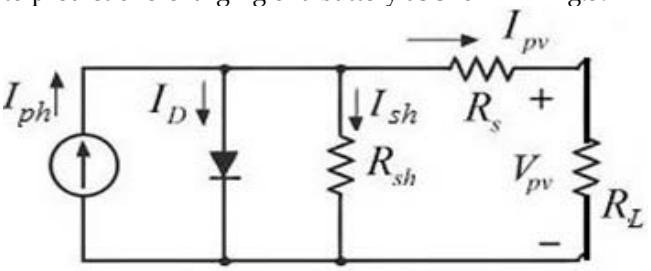

Fig. 4. Equivalent circuit of a solar cell

The above Fig.4 shows equivalent circuit of solar cell consists of single diode model, PV panel is designed for specific rating by using the following equations, by applying KCL to the above circuit we get,

$$I_{PV} = I_{Ph} - I_S - I_{rs} \quad (16)$$

$$I_{ph} = \left[I_{SC} + k_i\left(T_C - T_{ref}\right)\right]\left[\frac{S}{1000}\right] \quad (17)$$

$$I_{rs} = \frac{I_{SC}}{\left[\exp\left[\frac{qV_{OC}}{N_S kAT_C}\right]-1\right]} \quad (18)$$

$$I_S = I_{rs}\left[\frac{T_C}{T_{ref}}\right]^3\left[\exp\left(\frac{qE_g\left(\frac{1}{T_{ref}}-\frac{10}{T_C}\right)}{kA}\right)\right] \quad (19)$$

$$I_{pv} = N_P I_{ph} - N_p I_S \times\left[\exp\left(\frac{q\left(V + I\,R_S\right)}{N_S AKT_C}\right)-1\right] \quad (20)$$

Here,

I_{ph} -light generated current.

I_S =Diode saturation current.

I_{rs} =Reverse saturation current.

I_{pv} = Output current of PV-cell.

3 Block Diagram Representation of Single-Phase Microgrid System

The block diagram representation of 1-ϕ microgrid system uses proposed control algorithm as shown in Fig.5. In this microgrid consists of micro hydro driven SEIG, PMBLDC driven by wind turbine, solar PV array generation and BESS.

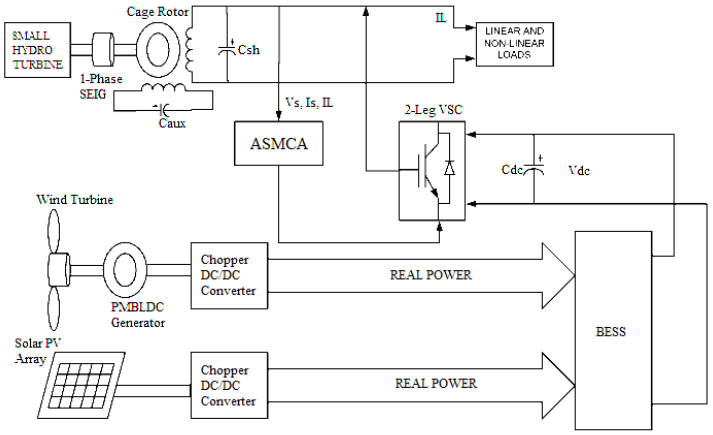

Fig. 5. Block diagram representation of 1-ϕ microgrid

Among all the renewable energy sources, micro-hydro system which generates AC power and directly caters to the load. Remaining two generating sources generating DC power, which is connected to load via voltage source converter. If the generation of conventional energy source is less than the demand at that instant non-conventional energy sources supplies the additional power through VSC to load. If all three generating sources is less than the demand, at that instant BESS comes in to the action to compensate the additional power to require demand of the load.

4 Adaptive Sliding Mode Control

An adaptive sliding mode control based algorithm is developed to estimate the reference source current and switching pattern for VSC of microgrid. The block diagram of proposed ASMCA is shown in Fig. 6. Under varying load conditions to maintain the PCC voltage at reference value.

The magnitude of terminal voltage of the single-phase SEIG is estimated as,

$$V_t = \sqrt{v_p^2 + v_q^2} \quad (21)$$

Where v_p and v_q are the in-phase and quadrature constituents of the microgrid AC voltage. The quadrature constituent of microgrid AC voltage is estimated and generated using frequency estimation and phase shifting (FEPS) block.

The microgrid AC voltage may be expressed as,

$$v_p = V_t \sin \omega t$$

$$v_q = V_t \cos \omega \quad (22)$$

Where

v_p = instantaneous AC voltage,

v_t = amplitude of voltage

ω = angular frequency of the microgrid AC voltage.

The in-phase and quadrature unit templates of microgrid AC voltage are derived as,

$$u_q = \frac{v_q}{V_t}, u_p = \frac{v_p}{V_t} \quad (23)$$

The proposed control algorithm is a combination of two control loops. First loop controls its voltage by injecting an adjustable reactive power and other loop balances active power among various energy elements in the microgrid.

4.1 Estimation of In-Phase Part of Reference Source Current

The ASMC extracts active power part of load current as follows. If the,

$u_p(t)$ = in-phase unit template of microgrid AC voltage

$i_h(t)$ = harmonic current component, have equal frequency,

M_{p1} = multipliers output

X_p = consists of direct and alternative current (DC and AC) components.

$W_p(t)$ = real power weight component of load current.

M_{P2} = The output of an integrator

$i_{Lpf}(t)$ = Fundamental real power component of load current.

$$i_h(k) = i_L(k) - i_{Lf}(k) \quad (24)$$

The M_{p1} multiplier's output X_p at k_{th} sampling instant is as,

$$X_p(k) = u_p(k) i_h(k) \quad (25)$$

The output of integrator I_p at $(k+1)_{th}$ sampling instant is estimated as,

$$W_p(k+1) = W_p(k) + Au_p(k)\{i_L(k) - i_{Lpf}(k) - i_{Lqf}(k)\} \quad (26)$$

The error in system frequency at k_{th} sampling instant is estimated as,

$$x_1(k) = f^*(k) - f(k) \quad (27)$$

Where

f*(k) = reference frequency

f = system frequency.

The derivative of system frequency error is calculated as,

$$x_1 = x_2(k) = \frac{1}{T}\{x_1(k) - x_1(k-1)\} \quad (28)$$

$x_2(k)$ = derivative of the system frequency

$x_1(k)$ = error signal

Where x_1 and x_2 are the state variable of the system and T is the sampling interval.

The switching hyper plane function of the frequency loop of the ASMC algorithm is given as,

$$G = \zeta_1 x_1 + \zeta_2 x_2 \quad (29)$$

Where ζ_1 and ζ_2 are the gain constants of switching hyperplane function of the frequency loop.

G is a switching hyperplane function on the locus of active power constituent of the load and 1/Z represents a unit delay. The switching function is defined as,

a = +1 if $G_{X1}>0$

a = -1 if $G_{X1}<0$

b = +1 if $G_{X2}>0$

b = -1 if $G_{X2}<0$

P_{bal} = the power balance constituent

$$P_{bal}(k) = h_1 x_1 a + h_2 x_2 b \quad (30)$$

Where

h_1 and h_2 = gain constants of ASMC.

The amplitude of the real power constituent of the reference AC source current i_p^* is estimated as,

$$I_p^* = P_{bal} - W_p \quad (31)$$

The instantaneous active power constituent of reference source current is estimated as,

$$i_p^* = I_p^* * u_p \quad (32)$$

4.2 Estimation of quadrature Part of Reference Source Current

The Mq1multiplier's output X_q at K_{th} sampling instant is as,

$$X_q(k) = u_q(k) i_h(k) \quad (33)$$

The output of integrator I_q at $(K+1)_{th}$ sampling instant is estimated as,

$$W_q(k+1) = W_q(k) + Au_q(k)\{i_L(k) - i_{Lpf}(k) - i_{Lqf}(k)\} \quad (34)$$

Where,

$W_q(k+1)$ and $W_q(k)$ are the outputs of integrator I_q at $(K+1)_{th}$ and K_{th} sampling instants.

The voltage error in microgrid AC voltage at K_{th} sampling instant is given as,

$$V_{ter} = V_{tref}^*(k) - V_t(k) \quad (35)$$

The reactive power constituent of reference source current is calculated as,

The voltage error V_{ter} is calculated using (35) is processed in a PI controller used to control the microgrid AC voltage. The output of PI controller at K_{th} sampling instant is as,

$$I_Q(k) = I_Q(k+1) + k_{pb}\{V_{ter}(k) - V_{ter}(k+1)\} + k_{ib} V_{ter}(k) \quad (36)$$

Where

k_{pb} and k_{ib} = the proportional and integral gain constants of the PI controller employed for microgrid AC voltage control.

The amplitude of reactive power constituent of reference source current is estimated as,

$$I_q^* = I_Q - W_q \quad (37)$$

The reactive power constituent of reference source current is calculated as,

$$i_q^* = I_q^* * u_q \quad (38)$$

4.2 Estimation of total Reference Source Current

The total reference control current (is*) is estimated as,

$$\left(i_s^*\right) = I_p^* + I_q^* \quad (39)$$

This reference control current (i_s^*) is compared with sensed source current (i_s) to calculate the current error constituent as,

$$I_{ser}^* = i_s^* - i_s \quad (40)$$

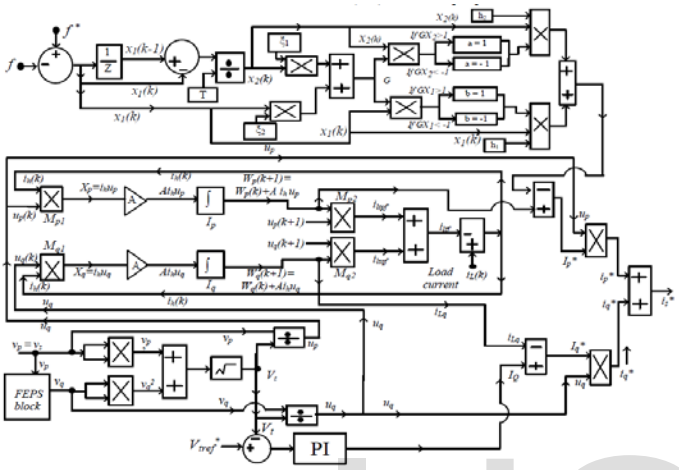

Fig. 6. Control algorithm of Adaptive Sliding Mode Control (ASMC)

5 Results And Discussion

This section presents the results of dynamic performances of microgrid.

5.1 Dynamic Performance of Proposed Microgrid

The effect of change in insolation level of PV and step change in wind speed and load are taken into consideration to verify the dynamic performance of the proposed control.

5.1.1 Dynamic Performance of Proposed Microgrid at a Step Change in Solar Insolation Level

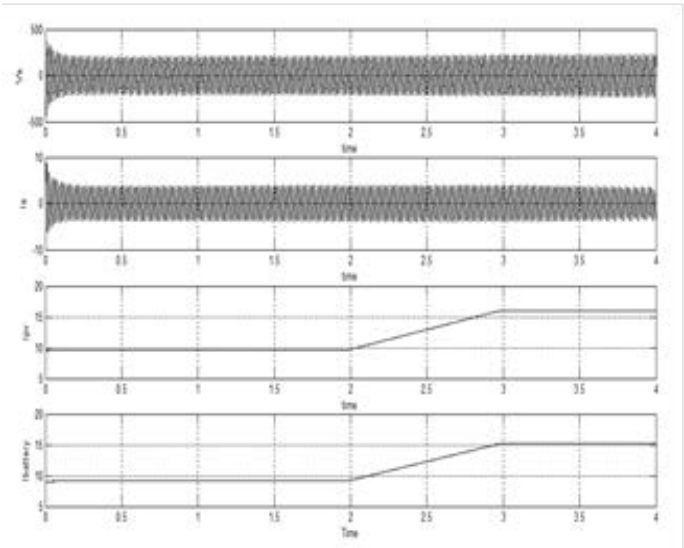

Fig. 7. Dynamic performance of the Vs, Is, Ipv and Ibattery, with the step increase in insolation level.

The dynamic execution of SEIG current is appeared in Fig. 7, with the progression increment in insolation level does not bring about any unsettling influence or change in stack current, as showed in Fig. 8. The dynamic execution of the framework voltage, SEIG present, sunlight based PV-exhibit current and battery current with the abatement in insolation level are shown in Fig. 9. The progression diminish in insolation level causes an abatement the sunlight based PV-cluster current with a similar incline and it therefore diminishes the battery current yet it doesn't exasperate the framework AC voltage, stack current or framework recurrence. The battery current goes from charging to releasing mode so as to recapture the power adjust in the framework as appeared in Fig. 9.

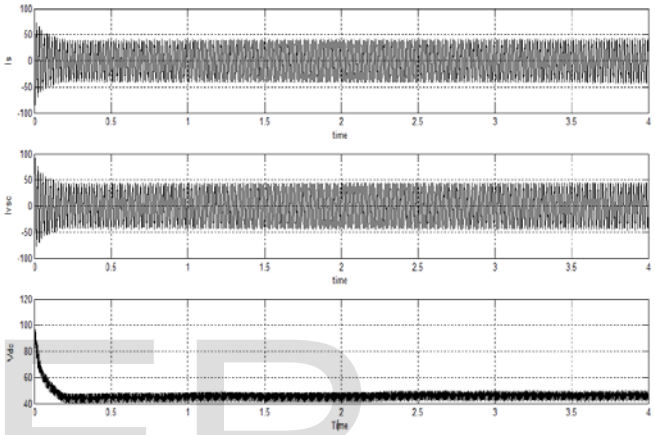

Fig. 8. Dynamic performance of IL, Ivsc, Idc with ASMC

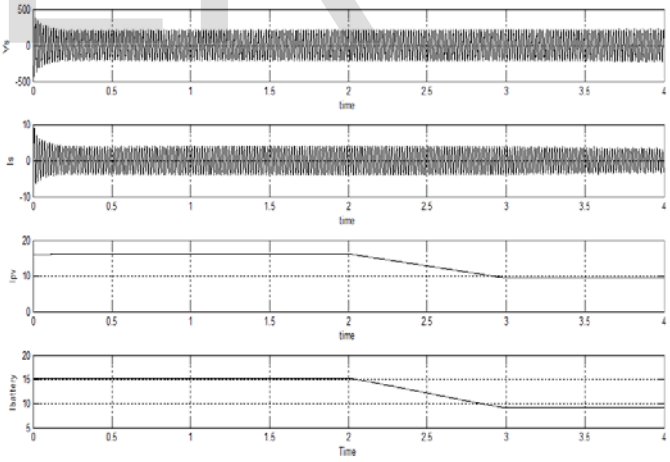

Fig. 9. Dynamic performance of step decrease in solar insolation level with ASMC

The outcomes demonstrate that in light of this progression increment in sun oriented PV-exhibit yield current, the controller builds the charging current of the battery to redirect the surplus produced energy to BESS so as to control the framework recurrence.

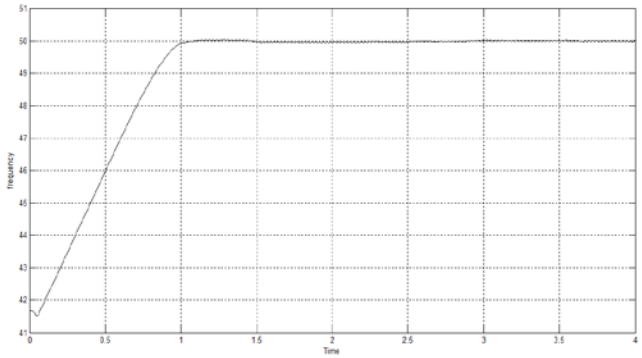

Fig. 10. Frequency responses under dynamic variation of insulation level changes

5.1.2 Dynamic Performance of Proposed Microgrid at a Step Change in wind speed

A step increment in PMBLDC generator current is seen in Fig. 11 while microgrid is following a stage increment in wind speed. Test outcomes appeared in Fig. 11 to Fig. 12 demonstrate the framework reaction to step increment in wind speed. The controller expands the battery charging current to redirect the surplus produced energy to the battery so as to control the framework recurrence. The dynamic reaction of framework AC voltage, SEIG current, PMBLDC generator current and battery current while the framework following a stage diminish in wind speed, is exhibited in Fig. 13. A stage diminish in PMBLDC generator current does not cause any unsettling influence in the SEIG current and framework AC voltage as appeared in Fig. 13.Test outcomes appeared in Figs. 11 and 12 demonstrate that aggregate produced control from each of the three sustainable sources turns out to be more than that of load, while the framework is following a stage increment in wind speed.

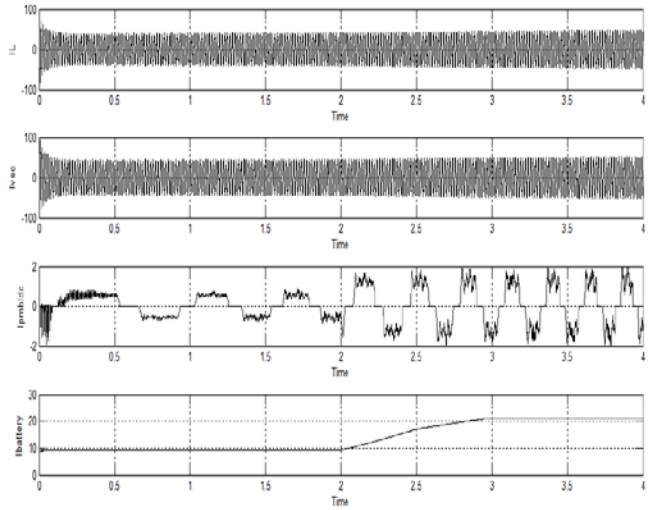

Fig. 11. Dynamic response of IL, iVSC, Ipmbldc and Ibattery, while the system is following a step increase in wind speed

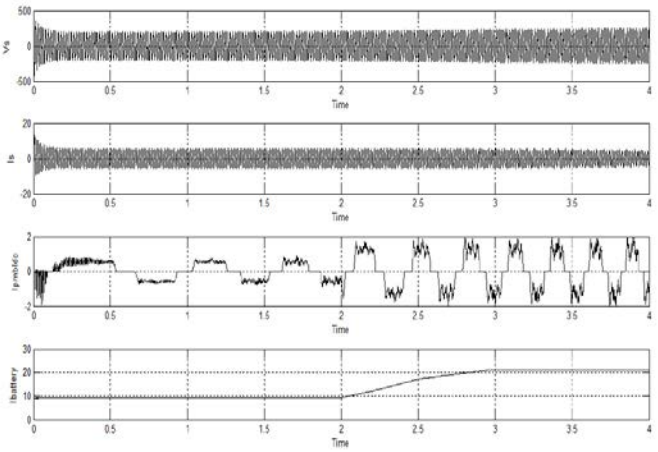

Fig. 12. Dynamic response of Vs, is, iPMBLDC and ibattery,

In this way, battery charging current increments to redirect surplus energy to the battery with a specific end goal to control the frequency and voltage. Fig. 12 exhibits the directional difference in battery current from releasing to charging mode because of a stage increment in PMBLDC generator current. This adjust of energy among the different vitality sources is accomplished utilizing recurrence circle of the control calculation. The progression increment in wind speed and PMBLDC generator current does not bring on any unsettling influence or change in stack current, as showed in Fig. 11. It can be seen from test comes about appeared in Fig. 13 that a stage diminish in wind speed causes a reduction in the PMBLDC yield current with a similar slant and it in this manner diminishes the battery current. While framework is following a stage diminish in wind speed, the battery enters releasing mode from charging mode keeping in mind the end goal to recover the power adjust in the framework as appeared in Fig. 13. A stage diminish in wind speed does not irritate the power quality parameters of the microgrid, for example, framework recurrence and voltage. It additionally does not cause any variety in the SEIG yield current and load current. It can be unmistakably seen from Fig.13.

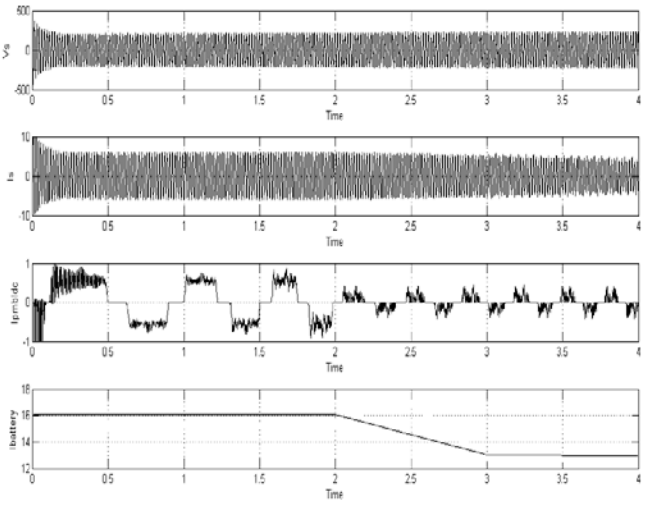

Fig. 13. Dynamic response of Vs, is, iPMBLDC and ibattery, while the

system is following a step decrease in wind speed

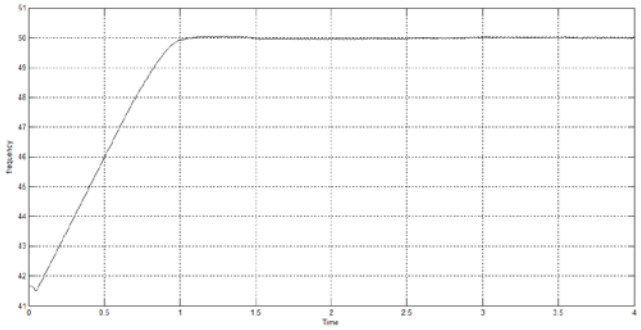

Fig. 14. Frequency responses under dynamic variation of wind speed changes

5.1.3 Dynamic Performance of the Microgrid, While it Following a Step Change in Load

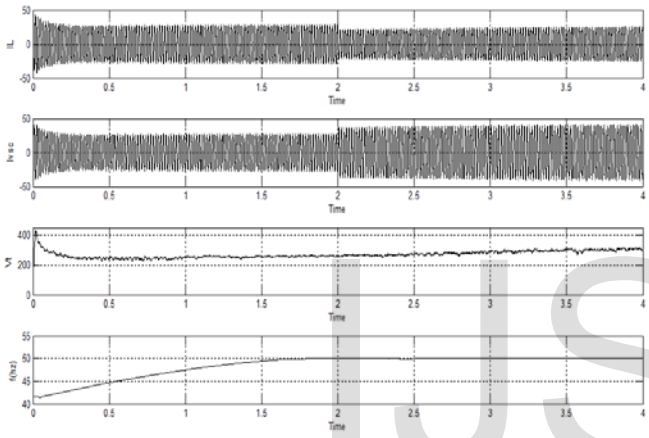

Fig. 15. Dynamic response of the proposed system, following a step change in wind speed and load

The dynamic reaction of the heap current, VSC current, SEIG yield voltage and framework recurrence while framework is following a stage change in stack is shown in Fig. 15. In this unique condition, the proposed control re-evaluates the reexamined symphonious and essential receptive power need of the SEIG and load and additionally dynamic power need of the heap with an amazing dynamic reaction. Here the control changes the exchanging design for VSC to remunerate the new responsive and dynamic forces need of the framework to direct framework voltage and recurrence, individually. Fig.15 demonstrates that microgrid voltage and recurrence are reestablished to their evaluated esteem quickly because of sudden change in stack.

6 Conclusions

The proposed SEIG based independent microgrid has incorporated the three sources, miniaturized scale hydro, sunlight based PV, and wind vitality. The ASMC calculation has been viable and has great control of the microgrid voltage and frequency. The proposed control calculation has likewise enhanced the power nature of the microgrid under straight and nonlinear burdens and furthermore guarantees the ideal use of BESS and sustainable power sources.

References

[1] P. Dondi, D. Bayoumi, C. Haederli, D. Julian, and M. Suter, "Network integration of distributed power generation," ***J. of Power Sources,*** vol.106, no. 1–2, pp. 1–9, 2002.

[2] J. P. Lopes, N. Hatziargyriou, J. Mutale, P. Djapic, and N. Jenkins, "Integrating distributed generation into electric power systems: A review of drivers, challenges and opportunities," ***Electric Power Syst. Research***, vol. 77, no. 9, pp. 1189–1203, 2007.

[3] I. Kumaraswamy S.Tarakalyani B. VenkataPrasanth Real time approch for enhacement of voltage stability using distributed generation. "34th International conference on recent innovations in engineering and technology (singapore), 19-August 2015,ISBN:978-93-85465-79- 6.

[4] H. Karimi, H. Nikkhajoei, and M. R. Iravani, "Control of an electronically-coupled distributed resource unit subsequent to an islanding event," ***IEEE Trans.*** *Power Del.*, vol. 23, no. 1, pp. 493–501, Jan.2008.

[5] I. Kumaraswamy B. VenkataPrasanth S.Tarakalyani, " Role of Distributed Generation in Voltage Stability Enhancement". ***International Journal of Current Engineering and Technology (IJCET)***,Vol:4,Issue 1, Feb2014,PP 60-64, ISSN 2347– 5161.

[6] F. Katiraei, M. R. Iravani, and P. W. Lehn, "Micro-grid autonomous operation during and subsequent to islanding process," ***IEEE Trans. Power Del.,*** vol. 20, no. 1, pp. 248–257, Jan. 2005.

[7] IEEE Standard for Interconnecting Distributed Resources with Electric Power Systems, 2003, ***IEEE Std.*** 1547.

[8] R. Zamora and A. K. Srivastava, "Controls for microgrids with storage: Review, challenges, and research needs," ***Renewable and Sustainable Energy Reviews,*** vol. 14, no. 7, pp. 2009–2018, Sep. 2010.

[9] A. Hajimiragha and M. R. D. Zadeh, "Practical aspects of storage modeling in the framework of microgrid real-time optimal control," in Proc. IET Conf. on Renewable Power Generat. (RPG), Sep. 2011, pp. 93– 98.

[10] F. Blaabjerg, R. Teodorescu, M. Liserre, and A. V. Timbus, "Overview of control and grid synchronization for distributed power generation systems," ***IEEE Trans. Ind. Electron.***, vol. 53, no. 5, pp. 1398–1409, Oct. 2006.

[11] A. Timbus, M. Liserre, R. Teodorescu, P. Rodriguez, and F. Blaabjerg, "Evaluation of current controllers for distributed power generation systems," ***IEEE Trans. Power Elect.***, vol. 24, no. 3, pp. 654–664, Mar. 2009.

[12] Claudio A. Cañizares and Rodrigo Palma-Behnke, "Trends in Microgrid Control," ***IEEE Trans. Smart Grid,*** vol. 5, no. 4, pp. 1905-1919, July 2014.

[13] U. K. Kalla, B. Singh and S. S. Murthy, "Normalised adaptive linear element-based control of single-phase self excited induction generator feeding fluctuating loads," in ***IET Power Electronics***, vol. 7, no. 8, pp. 2151-2160, August 2014.

[14] U. K. Kalla, B. Singh and S. S. Murthy, "Enhanced Power Generation From Two-Winding Single-Phase SEIG Using LMDT-Based Decoupled Voltage and Frequency Control," in ***IEEE Transactions on Industrial Electronics,*** vol. 62, no. 11, pp. 6934-6943, Nov. 2015.

[15] S. Gao, G. Bhuvaneswari, S. S. Murthy and U. Kalla, "Efficient voltage regulation scheme for three-phase self-excited induction generator feeding single-phase load in remote locations," in ***IET Renewable Power Generation,*** vol. 8, no. 2, pp. 100-108, March 2014.

[16] U. K. Kalla, B. Singh and S. S. Murthy, "Adaptive noise suppression filter based integrated voltage and frequency controller for two-winding singlephase self-excited induction generator," in IET ***Renewable Power Generation,*** vol. 8, no. 8, pp. 827-837, 11 2014.

[17] U. K. Kalla, B. Singh and S. S. Murthy, "Modified Electronic Load Controller for Constant Frequency Operation With Voltage Regulation of Small Hydro-Driven Single-Phase SEIG," ***in IEEE Transactions on Industry Applications***, vol. 52, no. 4, pp. 2789-2800, July-Aug. 2016.

[18] T. Esram and P. L. Chapman, "Comparison of photovoltaic array maximum power point tracking techniques," ***IEEE Trans. Energy Convers.***, vol. 22, no. 2, pp. 439–449, Jun. 2007.

[19] Z. Li, "Consistency between two adaptive detection methods forhar monic and reactive currents", ***IEEE Trans. Ind. Electron.,*** vol. 58, no. 10, pp. 4981–4983,2011